Behavior of GFRP Reinforced-Concrete Bubbled One-Way Slabs by Encased Composite Steel I-Sections

Mohannad Abdulkhaliq
Department of Civil Engineering, College of Engineering, University of Baghdad, Iraq
mohannad.abd2101m@coeng.uobaghdad.edu.iq (corresponding author)

Ali Hussein Al-Ahmed
Department of Civil Engineering, College of Engineering, University of Baghdad, Iraq
dr.ali-alahmed@coeng.uobaghdad.edu.iq

Received: 13 June 2024 | Revised: 23 July 2024 | Accepted: 3 August 2024

 DOI: https://doi.org/10.48084/etasr.8123

ABSTRACT

Bubbled Reinforced Concrete (RC) slabs have gained popularity in recent years as a practical construction method that eliminates unnecessary concrete in the center, thereby reducing the dead weight of the structure. This study provides a systematic framework to compare the performance and capabilities of one-way bubbled concrete slabs reinforced with Glass Fiber Reinforced Polymer (GFRP) bars and embedded steel I-sections. Four one-way concrete slabs, each with a length of 2,600 mm and a rectangular cross-sectional area of 600 mm in width and 150 mm in depth were employed. These slabs were reinforced with Glass Reinforced Plastics (GRP) rebar at the same reinforcement ratio and tested by two-point bending to failure. Different parameters such as specimen type (solid or bubbled slabs) and internal reinforcement were achieved using steel I-sections in two different shapes (2 and 4 pcs of steel I-sections), where 4I-section shape with a cross-sectional area equivalent to 2I-section shape, channel shear connectors, and bent steel bars (10 mm diameter) were used to improve the shear resistance. The results showed that bubbled slabs experienced a higher range of deformations (including deflection, strains, and cracks) by about (28%-88%) and a 15% decrease in ultimate load capacity compared to solid slabs. On the other hand, the use of steel I-sections as internal reinforcement significantly improved the specimen performance compared to unreinforced slabs (Steel Slab (SS) and Bubbled Slab (BS), respectively). Deflection was reduced by approximately 52% and 87% at the same load level, ultimate load capacity increased by approximately 121% and 179%, and flexural stiffness increased by approximately 197% and 272% at the same load level.

Keywords-Glass Fiber-Reinforced Polymer (GFRP) bars; embedded steel I-sections; bubbled slabs; flexural strength; one-way slabs; spherical voids; internal strengthening; deflection

I. INTRODUCTION

A slab is defined as a structural element consisting of a horizontal flat plate with parallel top and bottom surfaces. It is frequently employed as a floor or roof system in construction projects. A variety of structural elements may be deployed to support slabs, including columns, the ground, reinforced concrete beams, reinforced concrete walls, masonry walls, and structural steel members. The supporting elements provide the surface with stability and load-bearing capability [1-3]. A fundamental necessity for the construction of buildings is the use of blocks or slabs for the purpose of providing structural support. They create spaces within structures and necessitate the use of a considerable quantity of concrete. It is necessary to ensure that slabs are used and designed in an efficient manner in order to guarantee their stability and strength. The optimization of slab design has the potential to reduce the amount of concrete used, as the utilization of excess concrete may result in increased costs and the consumption of more resources [4, 5]. Previous research has demonstrated the feasibility of reducing the mass of concrete slabs without compromising their flexural strength. The aggregate interlock's shear resistance precludes the possibility of replacing the interior concrete in its entirety. In order to produce the compression block, it is necessary to reinforce the upper slab with concrete in order to provide the requisite flexural resistance. It is essential that the reinforcement be connected to the concrete in the slab's tension zone in order to provide the necessary flexural resistance. The bonding of the top and bottom faces ensures the transmission of stress and the cohesion of the slab [6-8]. BubbleDeck reduces the weight of the floor slab by removing the inner non-structural concrete. The core of the slab with void formers is 35% lighter. When

the dead load decreases, structural steel is used less for reinforcement. Lowering the dead loads in the foundation design reduces the construction time and usually results in cost savings [9-15]. The research and testing results indicate that slabs, including those with internal spherical spaces, exhibit flexural stiffness that is 87% of that observed in solid slabs. This suggests that a slab containing voids may exhibit greater flexibility or deformation at the serviceable point than a solid slab. Nevertheless, the ratio of stiffness to bending resistance determines deflection [16]. The use of steel-reinforced concrete in infrastructure has a history exceeding a century. However, in environments with hostile conditions, corrosion occurs rapidly, leading to structural collapse and the necessity for costly maintenance. Modern polymer technology has enabled the production of corrosion-resistant GFRP bars for use in structural concrete applications [17-23]. In recent years, GFRP bars have become an essential component in meeting the specifications for RC structures. This is due to their advantageous characteristics, including low weight, straightforward setup and management, corrosion resistance, and excellent tensile strength [24-33]. Despite its lightweight and cost-effective nature, the application of Fiber-Reinforced Plastic (FRP) remains constrained, regardless of its exceptional tensile stress resistance. To date, there have been few studies conducted on the use of FRP materials for the strengthening of bubbled slabs [34-37]. Authors in [37] investigated the effectiveness of GFRP sheets and elliptical balls in reinforcing bubble deck slabs under uniform stress. The application of a Finite Element Analysis (FEA) using the ANSYS software resulted in a reduction in slab deformation. The study included total, directional, and equivalent stresses for bubble deck slabs with and without GRP sheets. The numerical model employs 1,730×1,350×230 mm bubble deck slabs and an elliptical void measuring 180×240 mm. The use of GFRP sheets was found to reduce deflection and improve load carrying compared to bubble deck slabs with elliptical spheres only. The seven air-bubbled RC slabs (700×450×80 mm) were subjected to further analysis.

After burning and loading the slabs to failure, Carbon Fiber Reinforced Polymer (CFRP) strips were applied to hold them in place, except for one slab that was retained as a reference. The recovered bubbled slabs exhibited flexural strength equal to that of the reference specimen. In addition, their ultimate load was 79%-105% of the reference slab [38]. Further investigation revealed that the application of many layers of CFRP to the slabs resulted in improved resistance to external forces compared to the application of a single layer. Furthermore, the number of layers is inversely related to the amount of deflection [39]. Eindhoven University measured the flexural stiffness of bubbled slabs at depths of 230 and 450 mm. Experimental and theoretical research showed that bubbled slabs have different flexural properties than solid slabs. Darmstadt Technical University investigated the stiffness of a bubbled slab. A theoretical analysis and practical tests in the Netherlands confirmed the results. For the same strength, the bubbled slab has 87% of the flexural stiffness of a solid slab. The bubbles reduce the concrete volume of the solid slab to 66%. As expected, bubbled decks deflected slightly more than slabs [6, 40]. Authors in [41] evaluated the strength, performance, and long-term benefits of bubbled reinforced concrete slabs with plastic ball voids, testing fifteen 1,000 mm x 1,000 mm square reinforced concrete slabs and found that these slabs with a ball diameter to slab thickness ratio (B/H=0.51-0.80) have an ultimate load capacity of 90-100% of a similar solid slab. The use of lightweight concrete and GFRP composite bars to improve the durability and toughness of bridge deck slabs was examined, and concluded that lightweight concrete reduces the weight and cost of bridge construction over time [42]. Authors in [43] compared the use of GFRP reinforcement to steel reinforcement in areas prone to severe weather and magnetic fields. Seven slabs were analyzed in this study. One slab had steel reinforcement while the others had GRP rebar. The slabs were subjected to two-point bending. Reinforcement ratio and shear span to effective depth ratio were the main experimental parameters. The results disclosed that the GRP-reinforced slabs were bilinear elastic to failure, with higher loads confirming it. The effect of High-Strength Concrete (HSC) on the one-way shear efficiency of GFRP-reinforced concrete slabs was also examined. Twelve slabs were tested under four-point loading and it was found that HSC slabs had more extensive shear cracking, while NSC slabs had better shear stiffness [44]. Authors in [45] conducted experimental research on the effect of transverse thermal expansion of GFRP rebar on the structural performance of concrete slabs, six concrete slabs were constructed and tested with a two-point incremental load until failure, finding that temperature action can affect the concrete-GFRP bar bond, especially for larger bar diameters and low concrete cover values.

Prior research has demonstrated positive outcomes for conventional solid slabs and innovative bubbled slabs in unconventional slab systems, thereby encouraging the development of economical and effective systems. The objective of this study was to investigate the feasibility of combining GFRP bars as reinforcement with the voids in the bubbled slab system. This is due to the fact that GFRP materials possess a lower modulus of elasticity, lower stiffness, and weaker resistance to shear than steel. Similarly, the resistance to shear, flexural stiffness, and load-carrying capacity of bubbled slabs are inferior to those of traditional solid slabs. The primary objective was to prevent shear failure due to voids, enhance shear resistance, and optimize structural performance by reducing weight with GFRP bars, which are lighter and stronger than steel. The goal is to provide outstanding structural performance in bubbled slabs. This leads to a reduction in the costs associated with reinforcement and foundations. A review of the literature reveals a paucity of studies investigating the behavior of bubbled slabs reinforced by GFRP bars with internal strengthening by embedded steel sections. Accordingly, this research aims to examine the behavior of a one-way concrete bubbled slab reinforced by GFRP bars with internal strengthening by embedded steel I-shapes. This study is guided by two main objectives: the first is to investigate the influence of GFRP reinforcement in bubbled slabs on the ultimate load, stiffness, and deformations, and the second is to illustrate the impact of strengthening through the use of a steel I-shape as internal strengthening in bubbled slabs. This strengthening technique can be applied to bubble slabs

from a variety of perspectives. Firstly, the requisite raw materials for implementation are readily available, with the option to produce strengthening I-sections based on the appropriate design measurements (built-up sections). Secondly, the installation process is straightforward and rapid, requiring minimal effort to be completed between the rows of balls. Conversely, the enhancement of bubble slab performance through the optimization of maximum load, deflection, stiffness, and shear resistance renders this technology a highly viable candidate for implementation.

II. EXPERIMENTAL WORK

The experimentation program entails the testing of three one-way concrete bubbled slabs and one solid slab, each of which is reinforced by GFRP bars. The slabs were prismatic in shape, with a rectangular cross-section, and had the following dimensions: 2,600 mm in length, 2,400 mm in span center-to-center of supports, 600 mm in width, and 150 mm in thickness. The tests were divided into two groups, as shown in Table I. The initial group consisted of two unreinforced reference slabs: one solid slab (devoid of bubbles) and one bubbled slab (denoted Solid Slab (SS2) and Bubbled Slab (BS2), respectively). The second group comprises internally strengthened bubbled slabs with steel I-shaped reinforcement. The first specimen in this group is (BS2-2I-SC), having two steel I-shapes in cross-section dimensions of (72×30×6) mm fixed between ball lines and with channel shear connectors (30×30×3) mm fixed on the top surface of the section. Although the other specimen is denoted by (BS2-4I-SC), it features four steel I-shapes with a cross-section dimension of (50×25) mm, the flange and web thickness is (5 mm) and (3 mm), respectively, having an equivalent cross-sectional area of the steel-2-I-shapes in specimen (BS2-2I-SC) and being fixed in the same way. Also, channel shear connectors (30×15×3) mm were fixed on the top surface of the steel I-sections. In addition, five pcs. of steel bent-up bars (310 mm in length) along the width of the specimens on each side were located near the supports at a distance (*d*/2).

TABLE I. EXPERIMENTAL SLAB DESIGNATION

Group	Designation of a slab	Characteristic	Dimensions of steel I-shapes	Shear reinforcement (Bent-up bar)
Group one	SS2	Solid slab (control)	---	---
	BS2	Bubbled slab (control)	---	---
Group two	BS2-2I-SC	The bubbled slab has 2 steel I-shapes with channel shear connectors.	(72×30×6) mm	5 PCS, Φ10 on each side near support (310 mm in length)
	BS2-4I-SC	The bubbled slab has 4 steel I-shapes with an equivalent cross-sectional area of 2I-shapes, with channel shear connectors.	(50×25) mm, flange thick = 5 mm, web thick = 3 mm	5 PCS, Φ10 on each side near support (310 mm in length)

A. Material Properties

1) Concrete

Slab specimens were produced using self-compacting concrete with a cylinder compressive strength of 45.43 MPa. The mixture is composed of Type I ordinary Portland cement, natural sand, coarse aggregate that has been crushed and has a maximum particle size of 10 mm, silica fume, stone powder, third-generation superplasticizer, and water. A total of six test samples, measuring 150 mm on each side and 150 mm in height, were acquired in the form of standard cubes. Additionally, six test samples, measuring (150×300) mm, were acquired in the form of standard cylinders. The objective was to ascertain the average compressive strength of the concrete.

2) GFRP Bars

The reinforcement of all concrete slabs was conducted using 6 mm diameter GFRP deformed rods, with the objective of enhancing the durability of the structure. As indicated in the manufacturer's specifications, the mechanical properties of these bars are: an ultimate tensile strength of 900 MPa, a modulus of elasticity of 46 GPa, a weight of 97 g/m, and a transverse shear strength of 150 MPa.

3) Steel I-Shapes

The construction of the built-up steel I-shape involves the welding of flat bars together to provide internal strength. The initial configuration was a 72×30×6mm structure comprising two 2I-shaped sections. The second form, measuring 50 mm by 25 mm, has a flange and web thickness of 5 mm and 3 mm, respectively. It is composed of four sections (4I-shapes) with a cross-sectional area equivalent to that of the form (2I-shapes), evidenced in Figure 1. The mechanical characteristics were determined using coupons from flat bar specimens of various thicknesses. The laboratory tests on these coupons demonstrated that their yield stress (454.8 MPa) is within the Grade 60 range, their ultimate strength (575.7 MPa), elongation (17.33%), and modulus of elasticity (259,000 MPa) are within the expected ranges for this material.

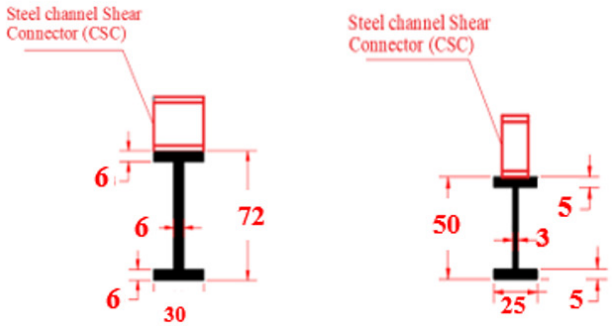

Fig. 1. Details of steel I-shapes.

4) Channel Shear Connectors (CSC)

In the production of channel shear connectors, the identical flat bars utilized in the fabrication of steel I-shapes were employed to create CSC, exhibiting the identical mechanical properties previously outlined. The CSC pieces were manufactured through the cutting and crooking of flat bars with

the use of specialized machinery. Two CSC specimens were manufactured with varying dimensions. The dimensions of the web, flange, and length for the initial specimen were 30 mm. The second specimen has a web height of 30 mm, a flange width of 15 mm, and a length of 30 mm. Both variants display a web thickness of 3 mm and a flange thickness of 3 mm.

B. Details of Specimens

The deformed GFRP reinforcing meshes were affixed to the upper and lower surfaces of the slab during the course of the testing procedure. Each mesh was composed of thirty-eight transverse bars, with a diameter of 6mm, and ten longitudinal bars, also with a diameter of 6mm. In accordance with the recommendations set forth in ACI 440.1R-15, a lower reinforcement ratio ($\rho f = Af / bd = 0.0037$) was employed to fulfill the requisite reinforcement requirements. Here, Af represents the area of GFRP reinforcing bars, b indicates the width of the slab, and d is the effective depth of the slab section. This ratio was in contrast to the ratio of balanced reinforcement (ρfb), which represents the under-reinforced case [46]. To ascertain the influence of varying parameters on the behavior of the control and strengthened bubbled slabs, three bubbled slabs and one solid slab were cast. The longitudinal and transverse spacing between bubbles in each bubbled slab is 115 mm. The details of the slab specimens are provided in Figure 2 and Table II.

TABLE II. DETAILS OF THE TESTED SPECIMENS

G	Designation	Thickness (mm)	Diameter of a sphere (mm)	Number of spheres	*D/H*	Reduction in self-weight ratio (%)	Distance between spheres *c/c*, (mm)	Type of internal strengthening
1	SS2	150	---	---	---	---	---	Un-strengthening
	BS2		90	95	0.6	15.48	115	Un-strengthening
2	BS2-2I-SC	150	90	95	0.6	15.48	115	Steel 2I-shapes
	BS2-4I-SC							Steel 4I-shapes

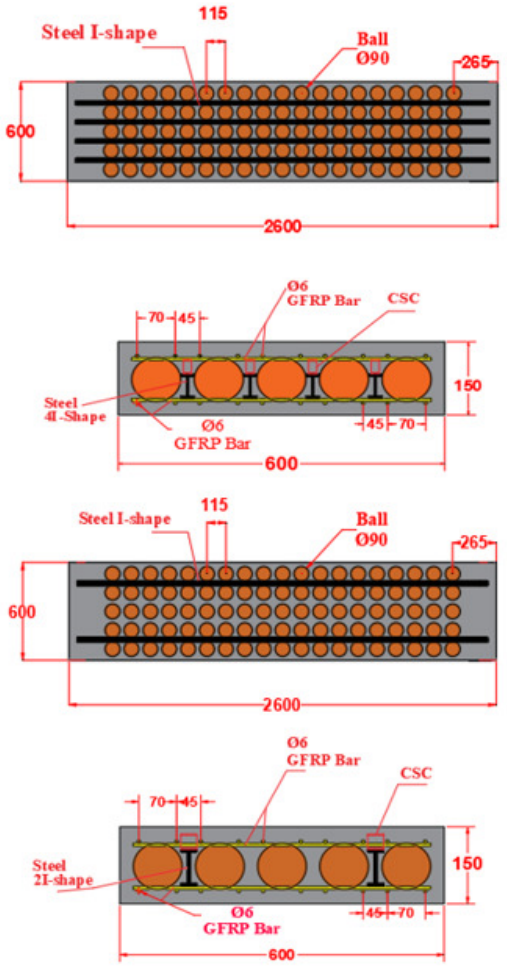

Fig. 2. Reinforcement and bubble distribution for bubbled slabs.

C. Preparation of Bubbled Slabs

The transverse GFRP bars were positioned at intervals that allowed for the ball diameter and center distance to be accommodated. For each bubbled slab specimen, 95 balls with a diameter of 90mm were used, resulting in a 15.48% reduction in self-weight. Subsequently, the balls were aligned with the square centers of the reinforcement mesh in the tension zone, thus preventing horizontal displacement. This was done with consideration of the ball's diameter and center distance. The reinforcing mesh was then transferred to the wooden mold and lifted to the requisite concrete cover using 22 mm plastic spacers. The bottom reinforcement mesh was secured to the wooden mold by a bolt and a series of tiny curved steel pieces. This configuration prevents the mesh from moving and ensures the desired 25mm side concrete cover is achieved. As previously described, a steel I-shape is formed by welding flat bars together. The CSC are manufactured by cutting and curving the flat bars to the specified dimensions using specialized machinery. Subsequently, the CSC pieces are affixed to a steel I-shape surface with a 90mm clear distance between them. For 2-I-shapes, a CSC with dimensions (30×30) mm is utilized, whereas an alternative CSC in the case of 4-I-shapes, each comprising 21 pieces of CSC, with dimensions (30×15) mm was employed. This was also the case for the 2-I-shapes. Subsequently, the steel I-shape, comprising CSC, is positioned and affixed between the longitudinal rows of balls and connected to the reinforcing mesh in the tension zone, thereby preventing horizontal movement. As a consequence, the compression zone top reinforcement mesh is installed above the balls, serving to prevent vertical movement. A plastic zip tie is utilized to connect the top and bottom reinforcement meshes. As shown in Figures 3 and 4, a bent steel bar (10 mm diameter) with a length of 310 mm is fitted between the two reinforcing meshes in five parts along the specimen's transverse direction near the supports to resist shear force. The steel bar has a diameter of 10 mm. In the experimental plan, all slabs were subjected to two-point bending until complete failure, with the shear span ratio (a) to an effective depth (d) ratio set at 6.4.

Fig. 3. Picture of the construction of test slabs.

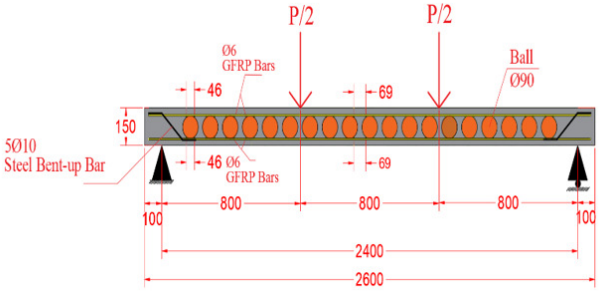

Fig. 4. Longitudinal cross-section in bubbled slab including steel Bent-up bar.

D. Test Instrumentation and Measurements

1) Load Measurements

The decision to paint the slabs white was taken in order to facilitate the observation of crack formation throughout the testing process. In this experimental setup, the slabs were positioned on two steel beams with a 2,400 mm spacing to provide lateral support. Following the 28-day casting period, each slab specimen underwent the requisite testing. Each slab was subjected to testing until failure using a hydraulic jack with a capacity of 500 kN. The specimens were subjected to two-point bending tests, with a load increment of 2 KN, until failure. Figure 5 presents the specifics of the testing apparatus. The construction of each slab was carried out in accordance with the standards set forth in ACI 440.1R-15 [46]. During this period, the deflections and crack development of the slabs were monitored at each load level.

2) Deflection Measurement

To quantify deflection, two Linear Variable Differential Transducers (LVDTs) and one dial gauge were employed to detect the deflection of the specimens. The LVDTs and dial gauge were situated at the midpoint of the slabs. As portrayed in Figure 5, the LVDTs and dial gauge have been securely attached to a supplementary steel frame.

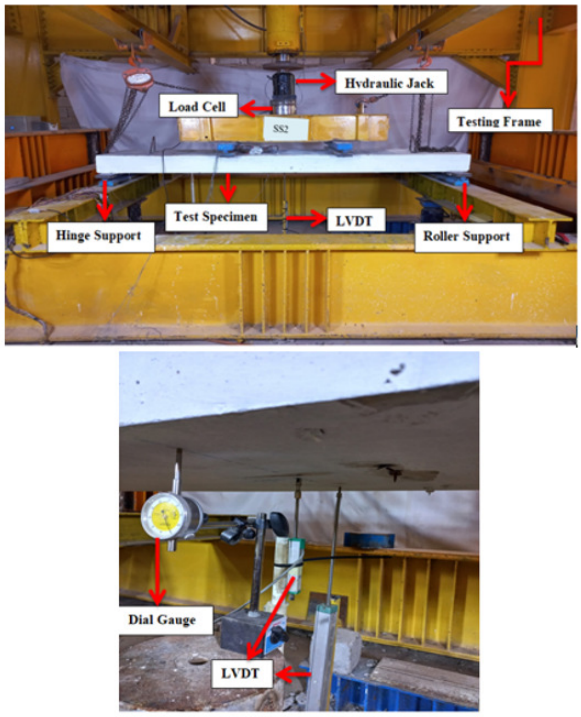

Fig. 5. Test specimen setup.

3) GFRP Strain Measurement

Two strain gauges with a gauge length of 5 mm were affixed at the center of the bottom GFRP mesh. The wires of the LVDTs were linked to either a data recorder or a strain indicator instrument, as shown in Figure 6. Specialized computer software was deployed to record four readings per second for each strain gauge and LVDT. This process was repeated until several readings had been acquired for every measurement. The resulting data were then subjected to statistical analysis and interpretation.

4) Steel Strain Measurement

To measure the strain in the steel, two strain gauges with a gauge length of 5mm were attached to each specimen, including I-shapes (2I-shapes and 4I-shapes). Each strain gauge was positioned in the center of the top fiber of the steel I-shape, as observed in Figure 6

5) Concrete Strain Measurement

Two strain gauges, each with a gauge length of 60 mm, were affixed to the concrete compression area of all slab specimens. These gauges were positioned at the midpoint of the top surface of the slabs, as exhibited in Figure 6.

III. RESULTS AND DISCUSSION

The study compares conventional and strengthened bubble slabs, employing a range of parameters, including first crack load (P_{cr}), mid-span deflection at the first crack (Δ_{cr}), deflection at 0.7 times the ultimate strength of SS2, the ultimate strength of the slab at failure (P_u), ultimate deflection at failure (Δ_u), and

the type and mode of failure. Table III presents the requisite parameters for the demonstration and comparison of the results.

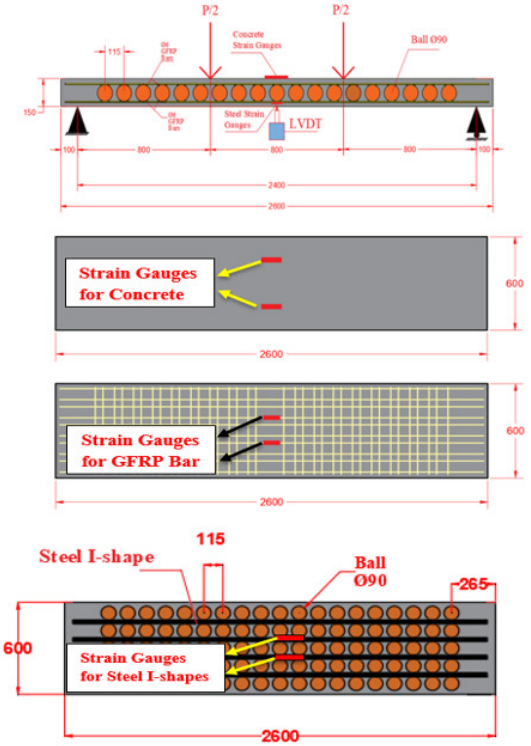

Fig. 6. Strain gauges location.

A. *Load-Deflection Curve*

The flexural failure of all four slabs is illustrated in Table III. Figure 7 presents a comparison of mid-span load and deflection. No cracking was observed in the slabs at the initial loading stage, resulting in a linear load-deflection relationship. This resulted in linear elastic deformation of the concrete and GFRP bars. The formation of cracks leads to a reduction in flexural stiffness. As the load increased, cracks began to form, which resulted in a reduction in the slab's flexural stiffness. The slab exhibiting flexibility (BS2) demonstrated a greater deflection than the other specimens. The presence of plastic balls within an inadequately reinforced BS2 matrix serves to diminish the slab's stiffness and augment its deflection, particularly when compared to solid slabs subjected to an equivalent load. Figure 7 shows that the slab designated SS2 exhibits greater stiffness than the slab designated BS2. The flexural deflection is a function of the service load. The results of the research indicate that the service load (Ps) accounts for approximately 70% of the ultimate load (SS2) of the reference solid slab. Therefore, it can be concluded that (Ps) = 91.21 kN. At this load, the control bubbled slab (BS2) exhibited a deflection of 75.43 mm, which was 42% greater than that of the solid slab. The results demonstrated that the bubble slabs with internal strengthening exhibited superior performance. The application of I-shaped strengthening steel resulted in an enhancement of stiffness relative to that observed in the SS2. The incorporation of steel I-shapes serves to augment the specimen's inertia. Consequently, the deflection is reduced. The bubbled slab specimen (BS2-2I-SC) manifested a stiffness that was 18% and 54% greater than that of SS2 and BS2, respectively. The specimen (BS2-4I-SC) showcased a stiffness that was 37% and 78% greater than that of SS2 and BS2, respectively. The statistical analysis revealed that the specimen (BS2-4I-SC) exhibited a 16% increase in stiffness compared to the specimen (BS2-2I-SC). Furthermore, the strengthened bubbled slabs demonstrated a lower deflection than both the reference SS2 and the BS2 under slab service load conditions. The BS2-2I-SC and BS2-4I-SC specimens exhibited 77% and 81% less deflection, respectively, in comparison to the SS2 specimen. The specimens displayed 84% and 87% less deflection than the reference specimen (BS2), respectively.

TABLE III. LOAD AND DEFLECTION COMPARISON FOR ALL TESTED SPECIMENS

Designation of a slab	P_{cr} (KN)	Δ_{cr} (mm)	Δ at 0.7, Pu of SS2 (mm)	P_u (KN)	Δ_u (mm)	Type of failure	Failure mode
SS2	27	4.1	53.07	130.3	84.78	Flexural tension failure	Brittle (GFRP-rupture)
BS2	20	3.95	75.34	110.91	90.63	Flexural tension failure	Brittle (GFRP-rupture)
BS2-2I-SC	53	6.79	12.07	288.64	79.81	Flexural compression failure	Brittle (concrete-crushing)
BS2-4I-SC	44	4.86	9.82	309.92	68.08	Flexural compression failure	Brittle (Concrete crushing)

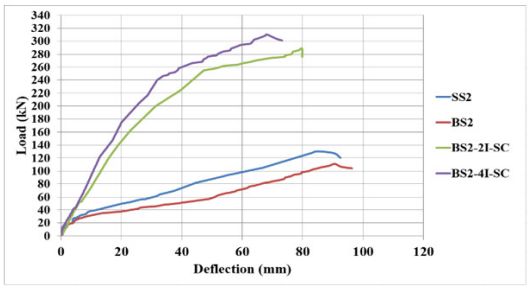

Fig. 7. Load vs. mid-span deflection of all tested specimens.

B. *Crack Pattern and Mode of Failure*

1) *General Behavior of Conventional Bubbled and Solid Deck Slab*

The SS2 and BS2 panels, when subjected to flexural loading, exhibited damage in the bending zone, manifesting as flexural cracks at the peak moment. Upon the application of a load of 27 KN, a fracture was observed to occur in the lower surface of the control SS2. A fracture was observed in the control bubbled slab at a loading of 20 kN. As the loads increased, the cracks propagated and ascended vertically. Additional cracks emerged in the same region. As the loading increased, the cracks propagated vertically and accelerated,

reaching the compression zone at 105 kN for the control SS2, and 83 kN for the control BS2. This led to a failure of the specimens at their maximum load capacity. When subjected to a stress level below that of the control slab (SS2), the bubbled slab samples exhibited a higher propensity for cracking. The presence of bubbles results in the removal of a considerable amount of concrete, which in turn reduces the specimen's stiffness and moment of inertia. The failure of GFRP-rebar led to flexural failure in the tension zone, as observed in the first group of specimens, which included the control models, namely SS2 and the BS2. As shown in Figure 8, the GFRP rebars exhibited rupture at the base of both the solid slab and the bubble slab, indicative of a brittle failure mode. Subsequently, the concrete was crushed. The failure mode and crack pattern of each specimen are presented in Figure 9.

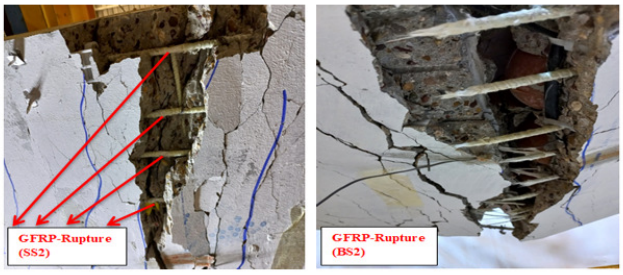

Fig. 8. Rupture in GFRP-bars in specimens SS2 & BS2.

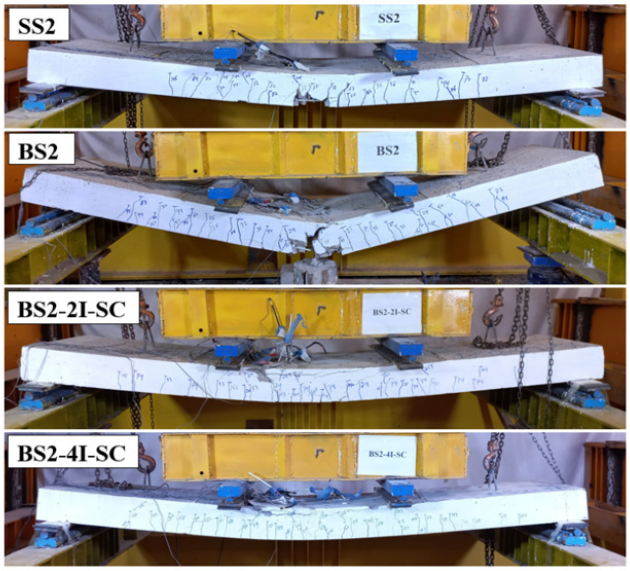

Fig. 9. Cracks pattern and mode of failure for each investigated specimen.

2) General Behavior of Strengthened Bubbled Deck Slab

The study revealed that the incorporation of internal steel I-shapes into the construction of bubbled slabs led to a notable enhancement in their overall strength. The second group of specimens exhibited noteworthy improvements in the ultimate strength, stiffness, crack pattern, and deflection. The initial fracture occurred at a load of 53 kN and 44 kN for the (BS2-2I-SC) and (BS2-4I-SC) specimens, respectively. The augmented moment of inertia in the reinforced slabs was ascribed to the augmented moment of inertia of the steel I-shapes. The increased first cracking load for strengthened bubbled slabs exceeds that of the BS2 specimen by 54% and the SS2 specimen by 18%, indicating enhanced stiffness. The moment of inertia of these specimens is greater than that of SS2 and BS2 due to the combination of the moment of inertia of the steel I-shapes and that of the specimen. As the load increased, cracks began to spread. It is worth mentioning that cracks extended into the compression zone at loads of 200 kN and 216 kN for the (BS2-2I-SC) and (BS2-4I-SC) specimens, respectively. At a load of 68 kN, cracks began to propagate on both sides of the specimen. The occurrence of cracks in the strengthened concrete slabs was observed at a higher load than that observed in the SS2 and BS2 specimens, due to the same causes previously stated. The first group's control specimens (SS2 and BS2) were designed under reinforcement-tension control; however, the incorporation of steel I-shapes for internal strengthening serves to reinforce the tension zone. This increases the load resistance of the tension zone and changes the failure mode to compression. In the compression zone, the second group of strengthened bubbled slabs failed. The failure was caused by concrete crushing on the upper surface of the specimen between loads. The GFRP rebars did not rupture, but, instead, a brittle failure mode was observed, as the one evidenced by the concrete strains at maximum strain.

C. Ultimate Loads Capacity

The data presented in Figure 7 and Table III pertain to the maximum load achieved by the slab specimens. It is noteworthy that the strengthened bubbled slab (BS2-4I-SC) demonstrated the highest failure load among the other specimens. The ultimate load capacity of specimens (BS2-2I-SC) and (BS2-4I-SC) exhibited an increase of 121% and 137%, respectively, in comparison to specimen SS2. Furthermore, these specimens demonstrated an increase of 160% and 179%, respectively, in comparison to specimen BS2. The incorporation of voids, represented by an array of plastic balls in two directions, had the most pronounced effect on reducing the ultimate load capacity of the BS2 by 15% in comparison to the SS2. This can be attributed to the presence of voids in the specimen BS2, which results in a reduction of the moment of inertia and, consequently, a reduction in stiffness.

D. Load-Strain Curves

1) Concrete Strain

Two strain gauges were positioned on the upper surface of the specimens to assess the concrete's compressive behavior on average. Prior to the onset of crushing and cracking, the strain gauge readings were nearly negligible. Figure 10 shows that the strain increased in conjunction with the elevated applied loads until the concrete reached its maximum tensile strength and failed due to the formation of fractures. The strain variations observed in each slab were constrained by the SS2 service load (91.21 kN). The unsupported BS2 demonstrated the greatest strain, and was 29% greater than that experienced by SS2 at the same load. The presence of balls and concrete in BS2 resulted in a reduction in specimen stiffness relative to SS2. This makes the specimen BS2 exhibit greater flexibility. The strain

observed in the strengthened bubbled slabs (BS2-2I-SC and BS2-4I-SC) was found to be 40% and 68% less, respectively, in comparison to that observed in the BS2 slab. The moment of inertia of the steel I-shapes results in a stiffer behavior for the strengthened bubbled slab specimens. The stiffer bubbled slabs exhibit reduced deflection and enhanced rigidity. In comparison to the SS2 specimen, the BS2-2I-SC and BS2-4I-SC strengthened bubbled slabs displayed a reduction in strain of 23% and 59%, respectively. Table IV presents the strain values of all specimens at the ultimate and service stages, with a load of 0.7 times the ultimate SS2 capacity for concrete and GFRP-bar.

TABLE IV. ALL TESTED SPECIMENS' GFRP AND CONCRETE STRAIN AT SERVICE AND ULTIMATE LOADING

Slab designation	Ultimate load P_u (KN)	Avg. Strain at the service loading stage (0.7 P_u of SS2)		Avg. strain at the ultimate loading stage ($\mu\varepsilon$)	
		GFRP-bar ($\mu\varepsilon$)	Concrete ($\mu\varepsilon$)	GFRP-bar ($\mu\varepsilon$)	Concrete ($\mu\varepsilon$)
SS2	130.3	10,735.75	1,323.9	19,411.95	2,096.09
BS2	110.91	18,491.81	1,701.81	19,422.17	2,016.04
BS2-2I-SC	288.64	1,195.2	1,018.61	12,479.98	4,101.77
BS2-4I-SC	309.92	1,181.66	548.43	12,795.10	3,035.19

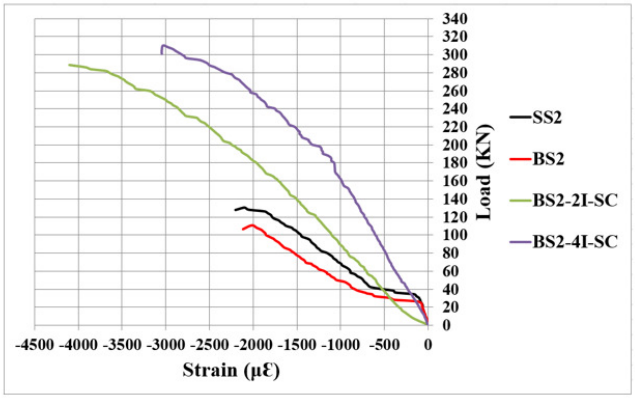

Fig. 10. Load-compressive Strain of concrete of all tested specimens.

2) *GFRP Strain*

Figure 11 illustrates the mean load-strain curve for two GFRP-bar longitudinal reinforcement tensile strains at the bottom mid-span. Similarly, the load-deflection behavior of GFRP reinforcement exhibits a bilinear load-strain relationship. A comparison was conducted between the bottom reinforcement strains of the first and second groups at the same loading stage, which was 0.7 times SS2. The analysis revealed that the unreinforced BS2 exhibited the highest strains. The strengthened bubbled slab specimens demonstrated significantly lower values than the non-strengthened slab specimens in the initial group (SS2 & BS2). The reduction in stiffness observed in the slab specimens can be attributed to the stiffening effect of the steel I-shapes. The presence of steel I-shapes resulted in a notable reduction in the strain experienced by the GFRP bars. The unreinforced BS2 exhibited a strain that was 72% greater than that of the SS2. The strain observed in the solid slab (SS2) is nine times greater than that evidenced in the strengthened bubbled slabs (BS2-2I-SC) and (BS2-4I-SC). The strain observed in the bubble slab (BS2) is 15 and 16 times greater than that detected in the strengthened bubbled slabs (BS2-2I-SC) and (BS2-4I-SC), respectively. The occurrence of maximum deformation was indicated by the continuous loading of the strengthened slab until its failure. Table IV presents the strain values for the concrete and GFRP-bar specimens at ultimate and service loads (0.7 *Pu* of SS2). The first-group reference slab specimens SS2 and BS2 demonstrated compliance with the GFRP-bar limitations. Figure 11 shows the rupture of the GFRP bars' bottom longitudinal reinforcement at mid-span. The experimental load-strain curves for each GFRP bar and concrete disclosed that the maximum strain of the GFRP bars corresponded to the manufacturer's datasheet value. The abrupt and brittle GFRP bar failure resulted in flexural failures in the first group.

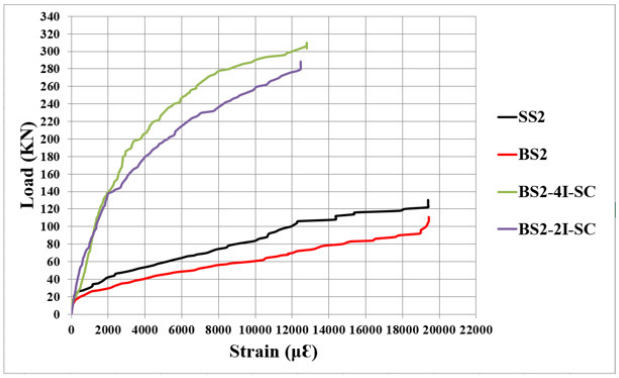

Fig. 11. Load-strain of bottom GFRP-bars.

3) *Steel I-Shapes Strain*

Figure 12 demonstrates the average load-strain curves as a function of applied loads for steel I-shapes at the mid-span of the top surface of the flange. Figure 6 presents the attachment of two strain gauges to the embedded steel I-shapes on the top flange at mid-span for two composite specimens (BS2-2I-SC and BS2-4I-SC). The mean value for each specimen was calculated. The ultimate tensile strain of composite specimens (BS2-2I-SC) and (BS2-4I-SC) was determined to be 1,843.7 at (288.64 kN) and 6,963 at (309.92 kN), respectively. Figure 12 illustrates that specimen (BS2-2I-SC) exhibits 58% less strain than specimen (BS2-4I-SC). The specimen (BS2-4I-SC) has a lower top surface, which results in greater operation within the tension zone than the specimen (BS2-2I-SC), which is closer to the NA. In specimens (BS2-2I-SC) and (BS2-4I-SC), the strains in the top flange of steel I-shapes exhibited a linear growth pattern up to the load of 150 kN and 190 kN, respectively, before transitioning to a steady growth pattern up to failure. The steel I-sections of specimen (BS2-4I-SC) reached a strain of 6,963, yet did not reach either the yield or plastic stages. A comparison of this specimen strain value with laboratory strain values for steel I-shapes confirms this. Table V depicts the steel I-shape strain at ultimate loading for strengthened bubbled slabs.

E. Flexural Stiffness of Slabs

The flexural stiffness of slabs is defined as the structural element's capacity to resist deformation resulting from bending forces. The slab's elastic modulus, moment of inertia, effective length, and boundary conditions all exert an influence on it. The flexural stiffness of slabs can be evaluated through the use of secant stiffness, which is determined by assessing the slab's load-deflection slope. The stiffness of a slab undergoes a rapid decline following the application of loads, due to the formation of cracks and inadequate bonding between the concrete and reinforcement bars.

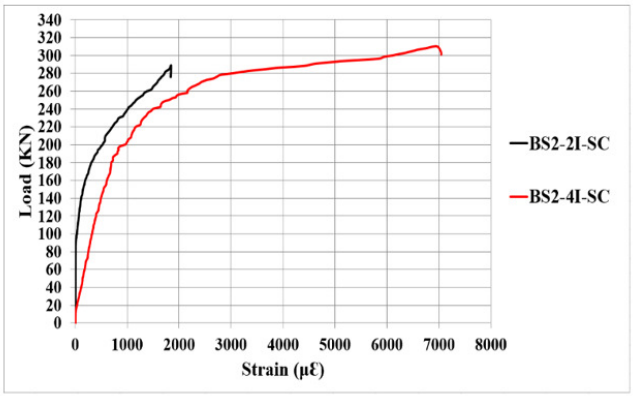

Fig. 12. Load-strain of top flange surface of steel I-shapes.

TABLE V. STRAIN OF STEEL I-SHAPES AT THE ULTIMATE LOADING STAGE FOR STRENGTHENED BUBBLED SLABS

Designation of a slab	Ultimate load P_u (KN)	Avg. Strain of steel I-shapes at ultimate loading stage ($\mu\varepsilon$)
BS2-2I-SC	288.64	1,843.70
BS2-4I-SC	309.92	6963

As portrayed in Figure 13, all K_u values are less than K_{cr}. The presence of voids within the slab, along with the associated reduction in flexural rigidity, may contribute to a reduction in stiffness at both the ultimate loading and cracking stages [47]. In order to determine the secant stiffness, (1) and (2) were employed:

$$K_{cr} = \frac{P_{cr}}{\Delta_{cr}} \quad (1)$$

$$K_u = \frac{P_u}{\Delta_u} \quad (2)$$

Table VI provides the estimated secant stiffness (K) at both the cracking and ultimate stages. The ratio of specimen stiffness exhibited fluctuations between the cracking and ultimate stages when the model characteristics were incorporated. The flexural stiffness of the specimen BS2 exhibited a decrease of 24% and 20% during the cracking (K_{cr}) and ultimate (K_u) loading phases, respectively, in comparison to the specimen SS2. This was attributed to the presence of voids resulting from the reduction in concrete volume due to the presence of balls. This led to a reduction in the moment of inertia of the bubbled slabs. Furthermore, the inherent lower stiffness of GFRP bars in comparison to their steel counterparts contributes to the overall stiffness of the model. The incorporation of steel I-sections as internal reinforcement in bubbled slabs markedly enhances their stiffness, as these sections augment the slab's moment of inertia. The second group of strengthened bubbled slab models (BS2-2I-SC and BS2-4I-SC) demonstrated a notable enhancement in stiffness at the cracking loading stage, exhibiting improvements of 54% and 78%, respectively, in comparison to the BS2 specimen. At the ultimate loading stage, these models displayed even greater stiffness, with improvements of 196% and 272% compared to the BS2 specimen, respectively. The second group of models (BS2-2I-SC and BS2-4I-SC) showcased enhanced stiffness, with increases of 18% and 37% during the cracking loading stage and 136% and 197% during the ultimate loading stage, respectively, in comparison to the SS2 specimen.

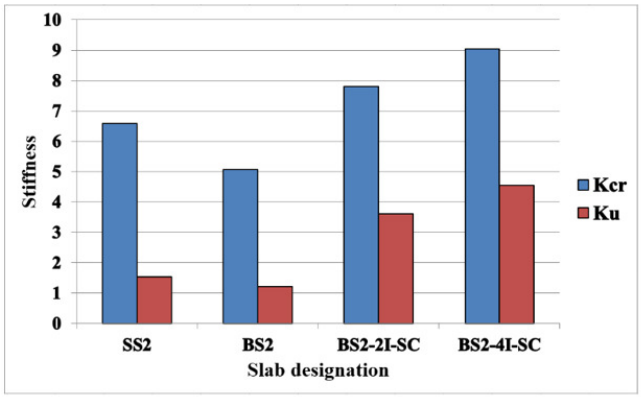

Fig. 13. Stiffness for all tested specimens at cracking and ultimate stage.

TABLE VI. STIFFNESS AT CRACKING AND ULTIMATE PHASE FOR ALL TESTED SPECIMENS

Designation of a slab	Cracking stage			Ultimate stage		
	P_{cr} (kN)	Δ_{cr} (mm)	K_{cr} (kN/mm)	P_u (kN)	Δ_u (mm)	K_u (kN/mm)
SS2	27	4.1	6.58	130.3	84.78	1.53
BS2	20	3.95	5.06	110.91	90.63	1.22
BS2-2I-SC	53	6.79	7.8	288.64	79.81	3.61
BS2-4I-SC	44	4.86	9.05	309.92	68.08	4.55

IV. LIMITS ACCORDING TO BRITISH REGULATIONS FOR BUBBLED SLABS

This section addresses the notable deficiencies associated with bubbled slabs, including their diminished shear strength, flexural stiffness, and rigidity factor when compared to solid slabs. The results of research and testing have demonstrated that the flexural stiffness of bubbled slabs is 87% that of solid slabs. This results in an increase in displacement during the Service Loading Stage (SLS). Given the elevated shear forces near the supports, to ensure adequate shear resistance, it is advisable to maintain a solid area around the columns or supports, as the concrete itself has a direct impact on shear resistance. In the design process, the shear strength of 60% of solid slabs is typically considered. Conversely, UK regulations stipulate that the stiffness factor for bubbled slabs should be set

at 0.88 for solid slabs. To ascertain how the findings of this study align with the limitations established by British guidelines for bubbled slabs, refer to Table VII. It is crucial to note that the British regulations only specify data for bubbled slabs that are reinforced with steel bars.

TABLE VII. COMPARISON BETWEEN UK LIMITATIONS FOR BUBBLED SLABS WITH EXPERIMENTAL

In % of solid slabs	UK standards for bubbled slabs reinforced by steel bars	Experimental results of bubbled slabs reinforced by GFRP bars	Notes
Flexural Stiffness	87%	80%	The reason behind this disparity is that compared to steel, GFRP is not as stiff.
Rigidity Factor	0.88	0.98	---
Shear Resistance	60%	75%	---

V. VALIDATION OF EXPERIMENTAL RESULTS FOR DISPLACEMENT BY USING FEA

The four slabs were subjected to two-point bending analysis using ABAQUS, resulting in scientifically robust findings. The findings of the FEA displacement were collated, classified, and presented for comparison with the results of the verification testing. The load-deflection relationship is presented in order to demonstrate these results. As revealed in Figures 14 to 17, the Finite Element Method (FEM) generates a more pronounced load-deflection curve for all slabs in comparison to the experimental results. The numerical and experimental curves of deflection under applied loads at the crack and service loading stages demonstrate that the Finite Element (FE) curves exhibit greater stiffness than the experimental curves. The following assumed elements in the FE analysis contribute to the observed variance in cracking and service loading: Initially, the concrete is devoid of shrinkage-induced air porosity and microcracks. However, the FEM assumes that concrete is homogeneous despite the presence of porosity and microcracks. In the context of the FEM, it is regarded that rebars are completely attached to concrete. Nevertheless, the bond-slip observed in real-world slabs would serve to diminish the composite effect between concrete and rebar. In the FEM, the modelling of two perpendicular GFRP bars at the same level leads to a stiffer mesh reinforcement than that achieved by joining metal wires. As demonstrated in the preceding section, the validation findings are deemed to be satisfactory.

VI. CONCLUSION

In this research, one-way bubbled concrete slabs reinforced with Glass Fiber Reinforced Polymer (GFRP) bars with embedded steel I-sections were tested for flexural behavior. Four-point static loading was applied to test the structural integrity of the specimens. Flexural characteristics such as cracking, deflection response to applied stresses, ultimate strength, and failure mechanism were evaluated.

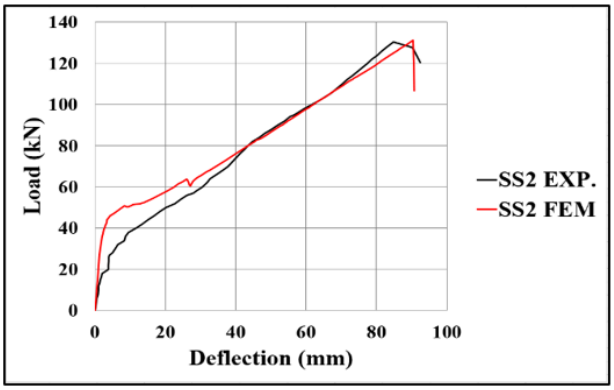

Fig. 14. FEM & EXP. Load-deflection curves of specimen SS2.

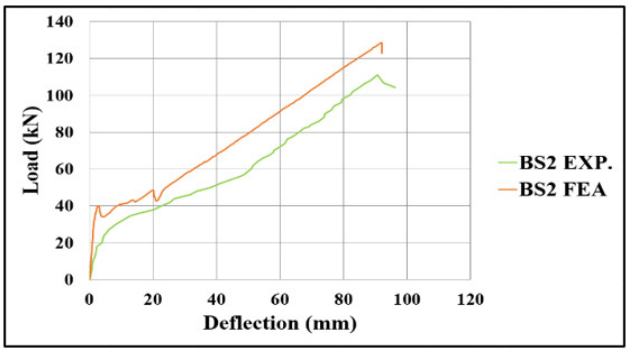

Fig. 15. FEM & EXP. Load-deflection curves of specimen BS2.

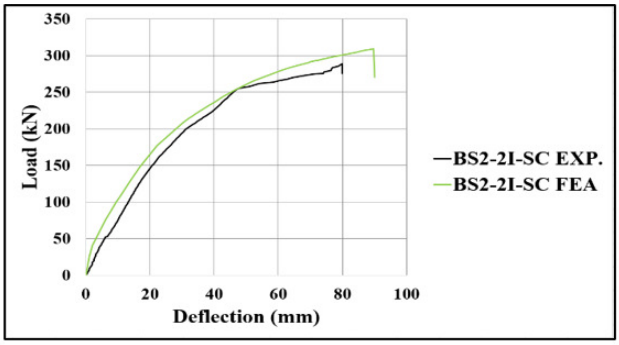

Fig. 16. FEM & EXP. Load-deflection curves of specimen BS2-2I-SC.

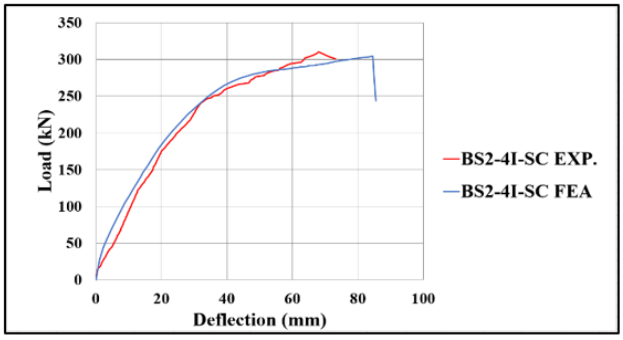

Fig. 17. FEM & EXP. Load-deflection curves of specimen BS2-4I-SC.

The following conclusions can be derived from the experiments of this research:

- The slabs tested and reinforced with GFRP bars exhibit bilinear behavior up to the point of failure.
- In the presence of balls, the unreinforced bubbled slab had 20% less stiffness than the solid slab once cracks formed at the ultimate stage due to the reduced moment of inertia. However, the reinforced bubbled slab specimens with two and four steel I-sections with the presence of Channel Shear Connectors (CSC) had 196% and 273% higher stiffness than that of the unreinforced bubbled slabs and 136% and 197% higher stiffness than that of the solid slabs, respectively.
- According to the study, unreinforced bubbled slabs had 15% less ultimate strength than that of thesolid slabs. Reinforced bubble slabs with two and four steel I-sections with CSC increased ultimate strength by 160% and 179%, compared to unreinforced bubble slabs, and 121% and 137%, compared to solid slabs, respectively.
- The presence of plastic spherical voids and Fiber-Reinforced Plastic (FRP) reinforcements resulted in an increase in the crack width and a decrease in the number of cracks. On the other hand, when bubbled slabs were strengthened, the number and width of maximum cracks decreased significantly.
- Internal reinforcement with steel I-sections prevented service cracking in the bubbled slabs. It also increased stiffness, load carrying capacity, flexural strength, first crack load, and shear strength.
- Compared to the solid slab specimen, the reinforced bubbled slab with two and four steel I-sections with CSC had 77% and 81% less deflection, respectively. In addition, the deflection was 84% and 87% less than the unreinforced bubbled slab specimen, respectively.
- The unreinforced slabs failed under flexural stress in the tensile zone. The failure mechanism was "brittle" as the GRP bars suddenly broke due to the design of the models (under reinforced tension control). Even though reinforced bubble slabs failed under flexural stress in the compression zone and the failure mode was considered "brittle" due to concrete crushing in the compression zone, the presence of steel I-sections as internal reinforcement changed the failure mode from tension to compression due to its contribution to strengthening and resisting stresses in the tension zone.
- Bubbled slab models strengthened with steel 4I shapes showed superior performance, reducing deflection and cracking, and increasing ultimate capacity, stiffness, and flexural strength compared to steel 2I-shapes.
- The shear strength of an unreinforced bubbled slab is 75% of that of a solid slab.
- Reinforced bubbled slabs with two or four pieces of steel I-sections with CSC revealed a 40% and 68% reduction in concrete compressive strain compared to unreinforced bubbled slab specimens.
- The first major achievement of the study was the reduction of self-weight by obtaining acceptable ultimate strength through the incorporation of plastic balls into slabs. Second, steel I-sections for internal reinforcement improved the deflection, stiffness, cracking, bearing capacity, flexural strength, and shear strength of the bubbled slab.

This study supports the usage of steel I-shapes to internally strengthen bubbled slabs and other structural parts. Moment of inertia for the Sections enhances slab stiffness, reduces deflection and cracks, and increases ultimate load capacity.

ACKNOWLEDGMENT

The authors express gratitude to the structural lab and engineering consulting bureau at Baghdad University/College of Engineering for their support in conducting experimental tests on concrete slab samples and investigating the materials used in the study, as well as the Department of Civil Engineering for their technical assistance.

REFERENCES

[1] A. S. Mahdi and S. D. Mohammed, "Structural Behavior of BubbleDeck Slab under Uniformly Distributed Load," *Civil Engineering Journal*, vol. 7, no. 2, pp. 304–319, Feb. 2021, https://doi.org/10.28991/cej-2021-03091655.

[2] A. H. A. Al-Ahmed, "Nonlinear Behavior of Self -Compacting Reinforced Concrete Two-Way Slabs with Central Square Opening under Uniformly Distributed Loads," *Journal of Engineering*, vol. 22, no. 7, pp. 35–54, 2016.

[3] A. S. Mahdi and S. D. Mohammed, "Experimental and Numerical Analysis of Bubbles Distribution Influence in BubbleDeck Slab under Harmonic Load Effect," *Engineering, Technology & Applied Science Research*, vol. 11, no. 1, pp. 6645–6649, Feb. 2021, https://doi.org/10.48084/etasr.3963.

[4] B. G. Bhade and S. M. Barelikar, "An experimental study on two-way bubble deck slab with spherical hollow balls," *International Journal of Recent Scientific Research*, vol. 7, no. 6, pp. 11621–11626, Jun. 2016.

[5] A. Gul *et al.*, "Experimental Study on the Structural Behavior of Cast in-situ Hollow Core Concrete Slabs," *Civil Engineering Journal*, vol. 6, no. 10, pp. 1983–1991, Oct. 2020, https://doi.org/10.28991/cej-2020-03091597.

[6] N. Oukaili and H. H. Yasseen, "Experimental Investigations on the Strength and Serviceability of Biaxial Hollow Concrete Slabs," *Journal of Engineering*, vol. 22, no. 11, pp. 36–54, Nov. 2016, https://doi.org/10.31026/j.eng.2016.11.03.

[7] C. C. Marais, "Design adjustment factors and the economical application of concrete flat-slabs with internal spherical voids in South Africa," Dissertation, University of Pretoria, 2010.

[8] N. Oukaili, H. Merie, A. Allawi, and G. Wardeh, "Reduced Volume Approach to Evaluate Biaxial Bubbled Slabs' Resistance to Punching Shear," *Buildings*, vol. 14, no. 3, Mar. 2024, Art. no. 676, https://doi.org/10.3390/buildings14030676.

[9] "Bubble Deck - Lighter Flat Slab Technology." https://www.bubbledeck-uk.com/.

[10] D. H. Al-Rashedi and A. H. A. Al-Ahmed, "Two-Way Bubbled Slabs Strengthened by Prestressing Strands," *IOP Conference Series: Materials Science and Engineering*, vol. 901, no. 1, Aug. 2020, Art. no. 012011, https://doi.org/10.1088/1757-899X/901/1/012011.

[11] A. V. Joseph, "Structural Behaviour of Bubble Deck Slab," M.Tech Thesis, St. Joseph's College of Engineering & Technology, Palai, 2016.

[12] T. Lai, "Structural Behavior of BubbleDeck* Slabs And Their Application to Lightweight Bridge Decks," Ph.D. dissertation, Massachusetts Institute of Technology, 2011.

[13] S. Calin and C. Asăvoaie, "Method for Bubbledeck Concrete Slab with Gaps," *Bulletin of the Polytechnic Institute of Jassy*, vol. 55, no. 59, pp. 63–70, Jan. 2009.

[14] V. Abishek and G. R. Iyappan, "Study on Flexural Behavior of Bubble Deck Slab Strengthened with FRP," *Journal of Physics: Conference Series*, vol. 2040, no. 1, Oct. 2021, Art. no. 012018, https://doi.org/10.1088/1742-6596/2040/1/012018.

[15] A. H. A. Al-Ahmed, F. H. Ibrahim, A. A. Allawi, and A. El-Zohairy, "Behavior of One-Way Reinforced Concrete Slabs with Polystyrene Embedded Arched Blocks," *Buildings*, vol. 12, no. 3, Mar. 2022, Art. no. 331, https://doi.org/10.3390/buildings12030331.

[16] *BubbleDeck Voided Flat Slab Solutions*. Jersey, UK: BubbleDeck, 2008.

[17] M. Abas Golham and A. H. A. Al-Ahmed, "Behavior of GFRP reinforced concrete slabs with openings strengthened by CFRP strips," *Results in Engineering*, vol. 18, Jun. 2023, Art. no. 101033, https://doi.org/10.1016/j.rineng.2023.101033.

[18] A. Wiater and T. Siwowski, "Serviceability and ultimate behaviour of GFRP reinforced lightweight concrete slabs: Experimental test versus code prediction," *Composite Structures*, vol. 239, May 2020, Art. no. 112020, https://doi.org/10.1016/j.compstruct.2020.112020.

[19] Y. Zheng, C. Li, and G. Yu, "Investigation of structural behaviours of laterally restrained GFRP reinforced concrete slabs," *Composites Part B: Engineering*, vol. 43, no. 3, pp. 1586–1597, Apr. 2012, https://doi.org/10.1016/j.compositesb.2011.11.012.

[20] A. Veljkovic, V. Carvelli, and M. Rezazadeh, "Modelling the bond in GFRP bar reinforced concrete thin structural members," *Structures*, vol. 24, pp. 13–26, Apr. 2020, https://doi.org/10.1016/j.istruc.2019.12.027.

[21] M. Zahid and S. Al-Zaidee, "Validated Finite Element Modeling of Lightweight Concrete Floors Stiffened and Strengthened with FRP," *Engineering, Technology & Applied Science Research*, vol. 13, no. 4, pp. 11387–11392, Aug. 2023, https://doi.org/10.48084/etasr.6055.

[22] W. Li, W. Huang, Y. Fang, K. Zhang, Z. Liu, and Z. Kong, "Experimental and theoretical analysis on shear behavior of RC beams reinforced with GFRP stirrups," *Structures*, vol. 46, pp. 1753–1763, Dec. 2022, https://doi.org/10.1016/j.istruc.2022.10.138.

[23] H. M. Mahdi and R. M. Abbas, "Torsional Behavior of CFRP Strengthening of SCC Box Beams with Web Openings under Repeated Loading," *Civil Engineering Journal*, vol. 9, no. 12, pp. 3038–3059, Dec. 2023, https://doi.org/10.28991/CEJ-2023-09-12-06.

[24] M. A. Adam, A. M. Erfan, F. A. Habib, and T. A. El-Sayed, "Structural Behavior of High-Strength Concrete Slabs Reinforced with GFRP Bars," *Polymers*, vol. 13, no. 17, Sep. 2021, Art. no. 2997, https://doi.org/10.3390/polym13172997.

[25] H. A. Hasan, H. Karim, H. A. Goaiz, A. M. Cabe, M. N. Sheikh, and M. N. S. Hadi, "Performance evaluation of normal- and high-strength concrete column specimens reinforced longitudinally with different ratios of GFRP bars," *Structures*, vol. 47, pp. 1428–1440, Jan. 2023, https://doi.org/10.1016/j.istruc.2022.11.056.

[26] S. A. Mohammed and A. I. Said, "Analysis of concrete beams reinforced by GFRP bars with varying parameters," *Journal of the Mechanical Behavior of Materials*, vol. 31, no. 1, pp. 767–774, Jan. 2022, https://doi.org/10.1515/jmbm-2022-0068.

[27] O. Abbas, "Evaluation of Deflection in High Strength Concrete (HSC) I-Beam Reinforced with Carbon Fiber Reinforced Polymer (CFRP) Bars," in *7th Asia Pacific Young Researches and Graduates Symposium*, Kuala Lumpur, Malaysia, Aug. 2015, vol. 16, pp. 519–533

[28] A. R. Murthy, D. M. Pukazhendhi, S. Vishnuvardhan, M. Saravanan, and P. Gandhi, "Performance of concrete beams reinforced with GFRP bars under monotonic loading," *Structures*, vol. 27, pp. 1274–1288, Oct. 2020, https://doi.org/10.1016/j.istruc.2020.07.020.

[29] S. I. Ali and A. A. Allawi, "Effect of Web Stiffeners on The Flexural Behavior of Composite GFRP- Concrete Beam Under Impact Load," *Journal of Engineering*, vol. 27, no. 3, pp. 76–92, Feb. 2021, https://doi.org/10.31026/j.eng.2021.03.06.

[30] A. Waleed and A. Al-Zuhairi, "Strengthening of RC Beam with Large Square Opening Using CFRP," *University of Baghdad Engineering Journal*, vol. 26, Nov. 2020, Art. no. 134, https://doi.org/10.31026/j.eng.2020.10.09.

[31] M. Y. Alabdulhady, M. F. Ojaimi, and A. H. Chkheiwer, "The efficiency of CFRP strengthening and repair system on the flexural behavior of RC beams constructed with different concrete compressive strength," *Results in Engineering*, vol. 16, Dec. 2022, Art. no. 100763, https://doi.org/10.1016/j.rineng.2022.100763.

[32] T. H. Ibrahim, I. A. S. Alshaarbaf, A. A. Allawi, N. K. Oukaili, A. El-Zohairy, and A. I. Said, "Theoretical Analysis of Composite RC Beams with Pultruded GFRP Beams subjected to Impact Loading," *Engineering, Technology & Applied Science Research*, vol. 13, no. 6, pp. 12097–12107, Dec. 2023, https://doi.org/10.48084/etasr.6424.

[33] M. A. Issa, A. A. Allawi, and N. Oukaili, "Performance of doubly reinforced concrete beams with GFRP bars," *Journal of the Mechanical Behavior of Materials*, vol. 33, no. 1, Jan. 2024, https://doi.org/10.1515/jmbm-2022-0308.

[34] F. H. Ibrahim and A. A. H. Al-Ahmed, "Strengthening of Cracked One-Way Reinforced Concrete Bubbled Slabs using External Strands," *Design Engineering*, no. 3, pp. 60–78, Mar. 2021.

[35] M. Reshma and P. Binu, "CFRP Strips on Punching Shear Strength Development of Bubble Deck Slab," *International Journal of Advanced Research Trends in Engineering and Technology (IJARTET)*, vol. 2, no. 9, Sep. 2015.

[36] M. Reshma and P. Binu, "Punching Shear Strength Development of Bubble deck Slab Using GFRP Stirrups," *IOSR Journal of Mechanical and Civil Engineering*, pp. 01–06, 2016.

[37] J. Jamal and V. Vijayan, "A Study on Strengthening of Bubble Deck Slab With Elliptical Balls by Using GFRP Sheets," *International Journal for Scientific Research and Development*, Apr. 2018, https://doi.org/10.2139/ssrn.3591289.

[38] W. A. Waryosh and H. H. Hashim, "Rehabilitation of Fire Damage Reinforced Concrete Bubbled Slabs," *Journal of Global Scientific Research*, vol. 1, pp. 278–288, Jan. 2020.

[39] S. S. Aman, B. S. Mohammed, M. A. Wahab, and A. Anwar, "Performance of Reinforced Concrete Slab with Opening Strengthened Using CFRP," *Fibers*, vol. 8, no. 4, Apr. 2020, Art. no. 25, https://doi.org/10.3390/fib8040025.

[40] *BubbleDeck Tests and Reports Summary*. Jersey, UK: BubbleDeck, 2006.

[41] W. D. Salman, "Flexural behavior of bubbled reinforced concrete slabs," PhD Thesis, University of Baghdad, 2012.

[42] T. Siwowski and A. Wiater, "Lightweight concrete bridge deck slabs reinforced with GFRP composite bars," *Roads and Bridges - Drogi i Mosty*, vol. 16, pp. 285–299, Jan. 2018, https://doi.org/10.7409/rabdim.017.018.

[43] S. Al-Tersawy and M. A. Ghanem, "Ductility and Flexural Behavior of One Way Concrete Slabs Reinforced With Local Gfrp Rebars: an Experimental and Analytical Study," *ERJ. Engineering Research Journal*, vol. 37, no. 1, pp. 95–106, Jan. 2014, https://doi.org/10.21608/erjm.2014.66873.

[44] A. Khavaran, "Effect of High-Strength Concrete on One-Way Shear Behavior of Concrete Slabs Reinforced with GFRP Bars," Jul. 2019, http://doi.org/10.13140/RG.2.2.14445.41445.

[45] O. El Zaroug, J. Forth, J. Ye, and A. Beeby, "Flexural Performance of Concrete Slabs Reinforced With Gfrp and Subjected To Different Thermal Histories," in *8th International Symposium on Fiber Reinforced Polymer Reinforcement for Reinforced Concrete Structures*, Patras, Greece, Jan. 2007.

[46] ACI Committee 440, *Guide for the Design and Construction of Structural Concrete Reinforced with Fiber-Reinforced Polymer Bars*. ACI, 2021.

[47] A. A. Al-Azzawi and S. H. Mtashar, "Behavior of two-way reinforced concrete voided slabs enhanced by steel fibers and GFRP sheets under repeated loading," *Results in Engineering*, vol. 17, Mar. 2023, Art. no. 100872, https://doi.org/10.1016/j.rineng.2022.100872.